Deposition, Characterization, and Enhanced Adherence of *Escherichia coli* Bacteria on Flame-Sprayed Photocatalytic Titania-Hydroxyapatite Coatings

Yuxin Liu, Jing Huang, Siyue Ding, Yi Liu, Jianhui Yuan, and Hua Li

(Submitted February 18, 2013; in revised form April 19, 2013)

Nanostructured titania has been extensively investigated as photocatalytic material and is capable of killing bacteria attached on its surface. The persistent challenge yet is how to effectively promote adhesion of bacteria on its surface for consequent extermination. The study presented here deals with liquid flame-sprayed nanostructured titania-hydroxyapatite (HA) coatings. Addition of HA alleviated phase transformation of titania from anatase to rutile during the coating deposition, reducing rutile to anatase ratio from 9.58 to 1.99%, and precluded effectively aggregation of the nano titania particles in the as-sprayed coatings. Adherence of *Escherichia coli* bacteria on the coatings showed significant dependence on content of HA, and the increased HA content resulted in enhanced attachment of the bacteria. Examination of the photocatalytic activity of the coatings through decomposition of methylene blue dye in water revealed that addition of HA did not markedly deteriorate the photocatalytic performances of the coatings. The coatings consisting of 10 wt.% HA showed the best photocatalytic activity, which is comparable to that exhibited by immobilized Degussa P25 coatings. The unambiguous evidence provided in this study suggests that the coatings made from combination of biocompatible HA and photocatalytic nano titania have great potential for antibacterium applications.

1. Introduction

Since the discovery of photo-induced cleavage of water on titania electrodes by Fujishima and Honda in early 1970s (Ref 1), titania has attracted intense attention for its high photo-reactivity, cheapness, nontoxicity and chemical stability (Ref 2). Development of titania as photocatalytic coatings achieved remarkable accomplishments and has been successful for environmental applications (Ref 3-5). Apart from its great potential for degrading toxic compounds, titania is claimed to have antibacterial properties as reported for the first time by Matsunaga et al. in 1985 (Ref 6). The highly reactive hydroxyl radical (·OH) derived from photocatalysis-triggered cleavage of H_2O serves as the main oxidant and is capable of inactivating microorganisms, including viruses, bacteria, spores, and protozoa (Ref 7). Addition of other materials, for instance, cerium (Ref 8), silver (Ref 9), etc., into nanosized

titania films has shown further enhanced bactericidal efficiency. Regardless of the extent to which the bacteria attached on the surfaces of photocatalytic titania are extinguished, contact, and subsequent attachment of bacteria on its surfaces, is essentially important for the overall elimination by titania. In most cases, TiO_2 can only decompose substances that come into contact, and this decomposing action fails to work while there is no impinging light (Ref 10). Taking into account the prerequisite of intimate contact between bacteria and the antibacterium material, the material must essentially favor the attachment of the bacteria. However, titania is basically bioinert material that cells/bacteria do not favor. Even though results from recent observation have indicated that titania in patterned nanostructures at its surfaces might offer favorable biocompatibility (Ref 11), further investigation is yet required to clarify if nano titania coating gives rise to enhanced attachment behavior of bacteria. In contrast, hydroxyapatite ($Ca_{10}(PO_4)_6(OH)_2$, HA) is known to have excellent adsorption properties as well as osteocompatibility (Ref 12) owing to its good affinity to proteins and lipids. Addition of HA into TiO_2 has been attempted to improve photocatalytic decomposition activity of the titania against bacteria, virus, pollen, and other biohazardous substances and chemicals (Ref 13). However, fabrication of nanostructured titania in particular titania-HA coatings/films remains challenging yet.

For photocatalysis applications, suspension of fine-powdered TiO_2 was investigated. However, several practical problems arise from the use of a catalyst in powder

Yuxin Liu, Jing Huang, Siyue Ding, Yi Liu, Jianhui Yuan, and **Hua Li**, Key Laboratory of New Marine Materials and Application Technology, Ningbo Institute of Materials Technology and Engineering, Chinese Academy of Sciences, Ningbo 315201, China. Contact e-mail: lihua@nimte.ac.cn.

form, for example, difficulty in the separation of the catalyst from suspension and aggregation of particles in suspension. For air purification, the only practical way in which the catalyst can be used is as a film (Ref 14). Since 1993, the idea of an immobilized photocatalyst on an inert support has begun to be widely accepted because it could help us eliminate the costly phase-separation processes (Ref 15, 16). Numerous techniques were reported for preparing supported titania, for instance, sol-gel (Ref 17-20), chemical vapor deposition (Ref 21-23), electrodeposition (Ref 24, 25), hydrothermal (Ref 26), and thermal spray. Thermal spray approach offers low cost, simplicity of operation, and capability of spraying a wide variety of materials (Ref 27), apart from the advantage of depositing coatings including multiple components. Furthermore, using liquid feedstock such as solutions or suspensions for thermal spraying yields higher flexibility in spraying nanosized particles and avoids effectively phase transformation from anatase to rutile. Suspension thermal spraying offers a large potential to fabricate efficient TiO_2 coatings (Ref 28-32) with favorable microstructural features such as certain porosity and specific surface, which are essential toward excellent photocatalytic performances.

Antibacterial TiO_2-HA composite coatings were deposited by using liquid flame spray technique in this study to provide the coatings with excellent bacteria adherent performances, substantial photocatalytic activity, and high anatase to rutile ratio. The contents of HA in the composite coatings were adjusted (10 wt.% HA, 30 wt.% HA, 50 wt.% HA), and the microstructural features of the coatings were elucidated. Even though usually a set of bacteria play together on the surfaces of photocatalytic materials, *Escherichia coli* has been widely used as the typical model for characterizing the photocatalytic performances of titania coatings. It is believed that the behavior of *E. coli* alone is able to give clear insight into typical adherence behavior of bacteria on the HA-containing titania coatings. Photocatalytic characteristics of the coatings and behaviors of *E. coli* bacteria on their surfaces were examined in this study.

2. Experimental Setup

2.1 Materials

304 stainless steel plates with the dimension of 40 mm × 25 mm × 2 mm in length, width, and thickness, respectively, were used as substrates. Anatase powders (99.9%, Aladdin, China) with an average size of 5-10 nm were employed for the coating deposition. HA was synthesized by wet-chemical approach, which was discussed in detail elsewhere (Ref 33). The HA suspension consisted of needle-like HA grains of ~200 nm in length and 20-40 nm in diameter. Bacterial adherence tests were performed against *E. coli* (ATCC 25922). Aqueous solutions of methylene blue (MB, Aladdin) with the concentration of 5 ppm were used as model pollutants for assessing the photocatalytic performances of the coatings.

2.2 Deposition and Characterization of the Coatings

A series of powders (pure TiO_2, TiO_2-10 wt.% HA, TiO_2-30 wt.% HA, TiO_2-50 wt.% HA, and pure HA) each with the weight of 3 g were suspended in 100 mL deionized water, and were mixed in an ultrasonic disintegrator for 10 min before spraying. The suspension after the ultrasonic treatment was then atomized by a spray gun. The suspension injector with a diameter of 1.5 mm was positioned just next to the flame torch, and the angle between the injector and flame was 30°. The pressure of the atomizing air was 0.7 MPa. The FS-4 flame torch (Wuhan Research Institute of Materials Protection) was employed for the coating deposition on the substrates sand blasted with working air pressure of 0.6 MPa. The flame spray parameters are given in Table 1. Phases of the samples were detected by x-ray diffraction (XRD, Bruker AXS, Germany) performed at a scanning rate of 0.1°/s using monochromatic Cu-Kα radiation operated at 40 kV. The chemistry of the coatings was further analyzed by x-ray photoelectron spectroscopy (XPS, AXIS Ultra DLD, Kratos). Hydrophobicity/hydrophilicity of the coatings was evaluated by measuring the contact angle of deionized distilled water droplet spread on their surfaces using a contact angle measurement instrument (Dataphysics OCA20, Germany). Electrostatic surface potentials of the coatings were measured by means of Veeco 3100 SPM (USA), and Pt-Ir coated Si probe was employed for the measurement. The XPS spectra of the typical composite coatings detected at their surfaces were recorded on a K-ALPHA spectrometer using an Al Kα monochromatized source. The constant energy pass was 50 eV. Spectra calibration was performed according to C1s level at 285 eV. The microstructural features of the powders and coatings were examined using field emission scanning electron microscope (FESEM, FEI Quanta FEG250, the Netherlands). Measurements of specific surface area of the coatings were made using the Brunauer, Emmett, and Teller (BET) method by adsorption of nitrogen gas on ASAP 2020 M apparatus at 77.3 K. The BET surface area was calculated over the relative pressure range of 0.05-0.20 MPa. For comparison purpose, Degussa TiO_2 (Evonik Degussa P25, 99.5%) coatings were also deposited and investigated in this study. The Degussa P25 powders were synthesized by Aerosil 200 process, and their average particle size was 21 nm. For the P25, the anatase-to-rutile ratio was about 80-20. The same spray parameters were used for P25 coating deposition.

Table 1 Liquid flame spray parameters

Oxygen gas pressure	0.5 MPa
Acetylene gas pressure	0.1 MPa
Acetylene gas flow	0.8 m^3/h
Spray angle	90°
Spray distance	20 cm
Suspension feeding rate	40 ml/min

2.3 Bacterial Adhesion Tests

Luria broth (LB) medium used in this study comprises 10 g tryptone, 10 g sodium chloride, and 5 g yeast extracted in 1 L water. After inoculation of a single colony of *E. coli* into the LB medium, the medium was shaken at 150 rpm for 24 h at 30 °C. The bacteria-containing LB medium was centrifuged at 2000 rpm for 5 min. After removal of supernatant, the bacteria were washed with phosphate-buffered saline (PBS) and were resuspended in PBS at a concentration of 5×10^7 CFU/mL. Then, 2 mL of the bacterial suspension was added to each well of a 12-well plate. The coating samples, anatase TiO_2, TiO_2-10 wt.% HA, TiO_2-30 wt.% HA, TiO_2-50 wt.% HA, HA, and P25-10 wt.% HA, were incubated in each well of the plate. The plate was incubated for 6 h at 30 °C before being rinsed with PBS to remove nonadherent bacteria. Then, the samples were fixed in 2.5% glutaraldehyde at 4 °C overnight, and finally rinsed twice in PBS. The samples were further dehydrated and critical-point dried by passing through a graded series of ethanol/water solutions at 25% (5 min), 50% (5 min), 75% (5 min), 90% (5 min), and 100% (2 × 10 min). Before SEM observation, the samples were air-dried and sputter-coated with gold. Enumeration of the attached cells was carried out by counting the cells from the SEM images. Digital images were taken randomly from at least five locations for each sample, and the number of the bacteria in each image was counted for averaged value.
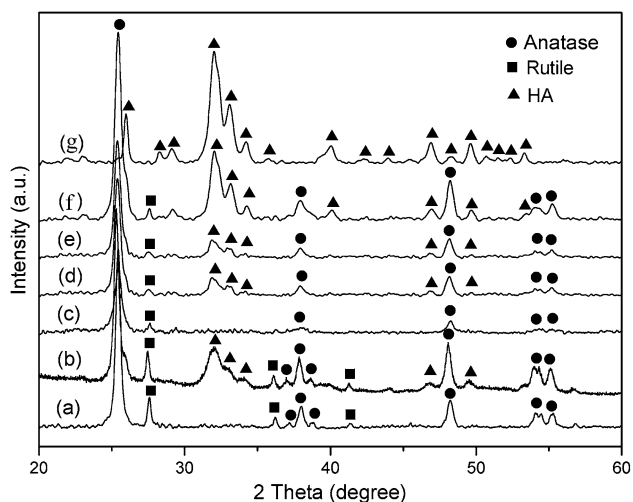
2.4 Assessment of Photocatalytic Performances

Photocatalytic activity of the coatings was evaluated by degradation of methylene-blue (MB) aqueous solution (30 mL, 5 ppm). Irradiation was produced by a 15-W UV lamp (PHILIPS, TLD15W BL) with the typical wavelength of 365 nm, and the distance between the UV light source and the coating samples was 15 cm. The variation of the MB concentration, as determined by the absorbance of the solution at 664 nm, was detected by a UV-Vis spectrophotometer (MAPADA, UV-3300 spectrophotometer).

3. Results and Discussion

3.1 Characterization of the Coatings

XRD detection shows that the anatase structure and crystalline HA were retained well in the coatings, apart from detectable rutile that resulted from transformation of anatase during the spraying (Fig. 1). Contents of the phases in the samples were quantified from their XRD spectra by means of the Rietveld refinement approach (Ref 34). The quantitative analyses of the phases (Table 2) show the highest content of rutile in the pure titania coating, with a rutile-to-anatase ratio of 9.58%. This ratio is much lower than those reported in titania coatings (Ref 35, 36), indicating that the liquid flame spray approach employed in this study is appropriate for deposition of nanostructured titania coatings with limited transition of anatase to rutile. Surprisingly, it can be found that with the increase of HA content from 0 to 50 wt.%, the ratio of rutile to anatase decreases from 9.58 to 1.99%. The phase information in particular HA content in the composite coatings was further detected by XPS. The XPS spectra of the titania-10 wt.% HA and titania-30 wt.% HA coatings are shown in Fig. 2, and the quantitative data are listed in Table 3. The magnified peaks for O1s (Fig. 2b) showed higher intensity at 529.46 eV (assigned to O^{2-}) for the titania-10 wt.% HA coating, indicating that the state of the oxygen in the titania-10 wt.% HA coating is primarily O^{2-} and that the oxygen in the titania-30 wt.% HA coating is mainly from OH^- (the O1s peak at 531.48 eV is assigned to OH^- (Ref 37)). This result is consistent with the XRD detection that the coating with 30 wt.% HA contains more HA. The stronger peaks for Ca2p (Fig. 2c) and P2p (Fig. 2d) at 347.74 and 133.83 eV,

Fig. 1 XRD curves of the liquid flame sprayed (a) pure P25 coating, (b) P25-10 wt.% HA coating, (c) pure TiO_2 coating, (d) TiO_2-10 wt.% HA coating, (e) TiO_2-30 wt.% HA coating, (f) TiO_2-50 wt.% HA coating, and (g) pure HA coating

Table 2 Content of anatase, rutile, and HA in the as-sprayed coatings

	Pure titania coating	Titania-10 wt.% HA coating	Titania-30 wt.% HA coating	Titania-50 wt.% HA coating	Pure P25 coating	P25-10 wt.% HA coating
Anatase	91.26 ± 1.20%	85.41 ± 1.26%	79.65 ± 1.45%	74.37 ± 2.16%	75.42 ± 1.38%	71.22 ± 1.67%
Rutile	8.74 ± 0.68%	6.93 ± 0.44%	3.93 ± 0.52%	1.48 ± 0.42%	24.58 ± 0.45%	20.55 ± 0.42%
HA	…	7.66 ± 1.02%	16.42 ± 1.10%	24.15 ± 0.81%	…	8.23 ± 0.97%
Rutile/anatase	9.58%	8.11%	4.93%	1.99%	32.59%	28.85%

respectively, suggest consistent result that HA in the 30 wt.% HA-containing coating is more than that in the 10 wt.% HA-containing coating. The binding energy of Ca2p is 347.74 eV, which agrees well with its values for HA (Ref 38). The XPS curves for Ti2p shown in Fig. 2(a) reveals the binding energy of 458.24 eV, being consistent with its values for titanium dioxide (Ref 39). It is noted that the Ca/P ratio is about 1.17 and 1.30 for the coatings (Table 3), which is apparently lower than the stoichiometric Ca/P molar ratio of HA (1.67). This is mostly likely attributed to minor phase transformation of HA to other phases, e.g., amorphous phase, tri-calcium phosphate, etc., during the coating deposition. The amorphous phase is evidenced by the broad peak located at ~32°, whereat the strongest crystalline HA peak is located. The undetectable XRD peaks for tri-calcium phosphate should be attributed to extremely low content of the phase in the coatings. It has been reported that addition of HA inhibited phase transformation of titania (Ref 40). It is likely that HA alleviates the evaporation of water during coating deposition, which consequently protects anatase particles from overheating. Direct experimental evidence is yet required to support the evaporation hypothesis. The lower content of rutile phase is expected to increase the photocatalytic

Fig. 3 Typical topographical and cross-sectional morphology of ▶ the titania-HA composite coatings showing very well retained nano titania spheres and needle-like HA grains, (a) pure titania coating, (b) titania-10 wt.% HA coating, (c) titania-30 wt.% HA coating, (d) titania-50 wt.% HA coating, (e) pure HA coating, (f) P25 coating, (g) P25-10 wt.% HA coating, and (h) typical cross-sectional morphology of the titania-10 wt.% HA coating showing the thickness of 20-30 μm. (The needle-like rods are HA grains, and the spherical particles are titania)

activity of the coatings (Ref 41, 42). Furthermore, it is noted that the actual content of HA in the coatings is lower than that in the starting feedstock. In general, spherical powders have better mobility than those having sheet-like shape. This in turn might result in higher

Table 3 XPS quantitative analysis results of the coatings

Coating sample	Peak	at.%	Ca/P ratio
Titania-10 wt.% HA coating	O1s	54.16	1.17
	Ca2p	6.72	
	P2p	5.74	
Titania-30 wt.% HA coating	O1s	50.93	1.30
	Ca2p	14.41	
	P2p	11.12	
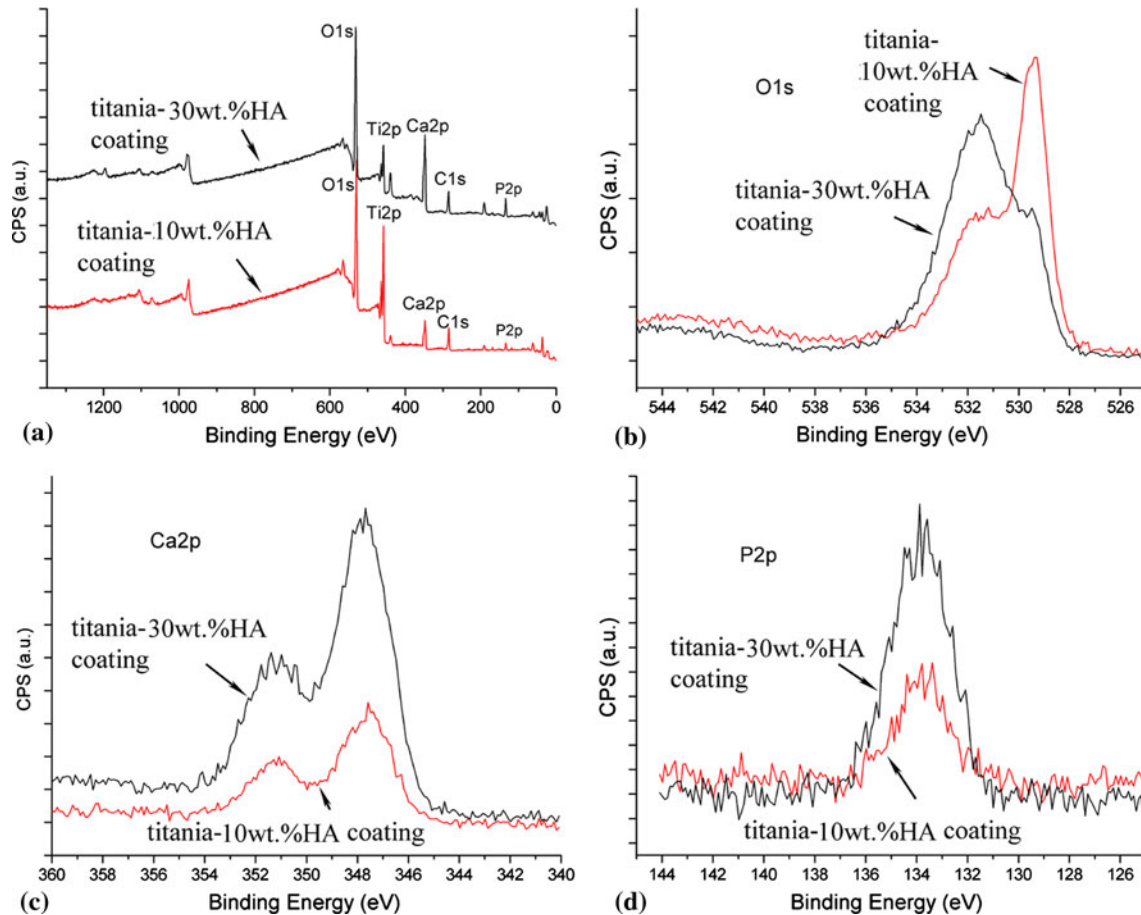
Fig. 2 XPS curves of the titania-10 wt.% HA coating and the titania-30 wt.% HA coating (a), the XPS curves for O1s, Ca2p, and P2p are shown separately in (b), (c), and (d)
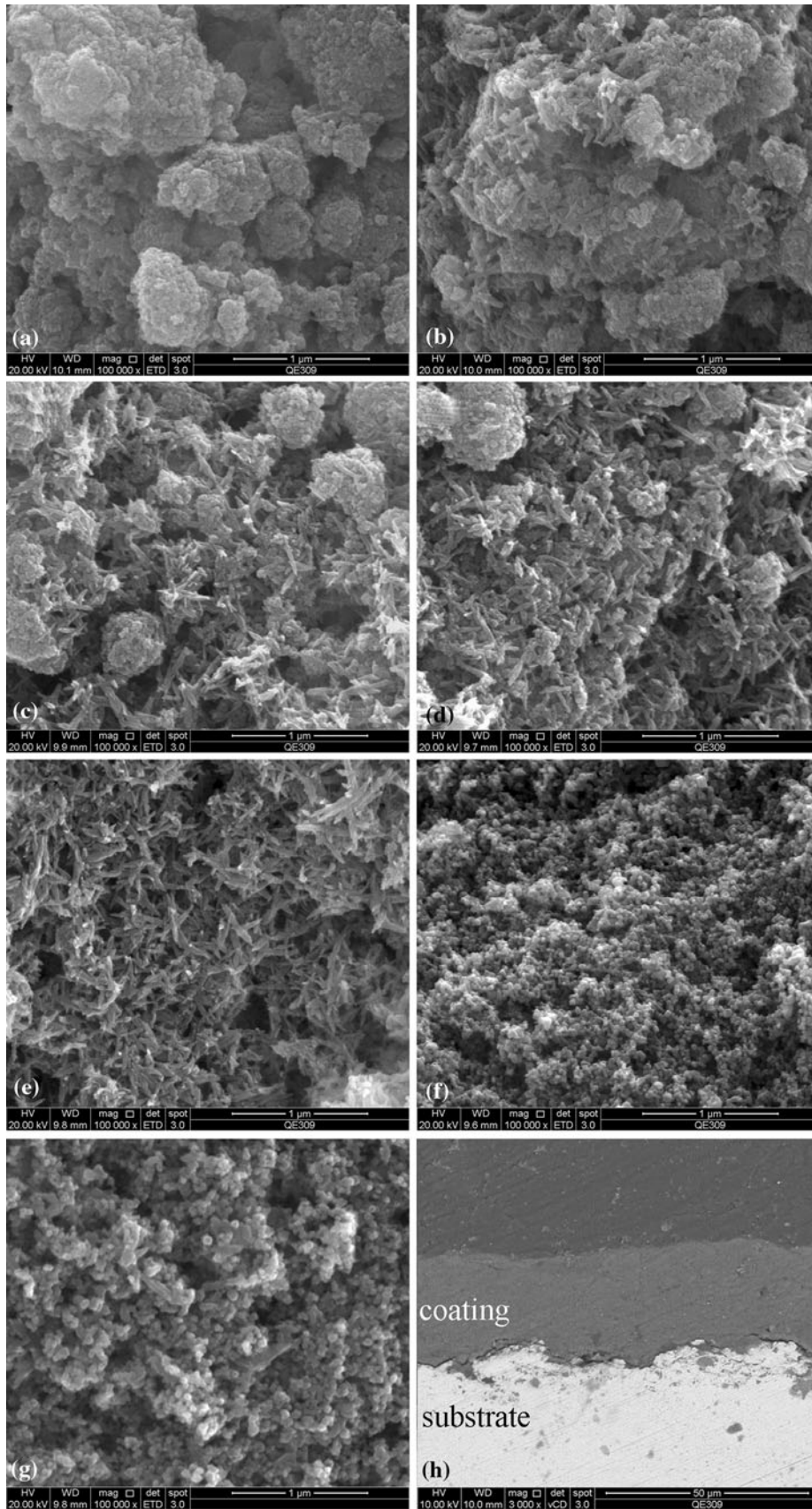
deposition rate of titania than HA, which needs further investigation.

SEM observation as shown in Fig. 3 reveals the topographical morphology of the coatings, that is, titania and HA retain their original morphological features with no signs of melting after the deposition. It clearly shows that titania particles are spherical with a diameter of 5-10 nm and HA grains have a needle-like shape with a length of ~200 nm. Mechanical interlocking among the needle-shaped HA and spherical titania particles most likely accounts for the bonding of the coatings. The thickness of all the coatings yields 10-20 μm which present dense structure as shown in Fig. 3(g). The titania particles in the pure titania coatings tended to aggregate into micron-sized particles (Fig. 3a) while needle-like HA in the pure HA coatings tended to aggregated into micron sheets (Fig. 3e). Increase in HA content is associated with decreased aggregation of the titania particles (Fig. 3b-d). It can also be observed that there are few aggregated HA sheets in the composite coatings (Fig. 3b-d). HA sheets may be destroyed into single needle or small groups by the micron-sized titania particles during ultrasonic treatment or spray processing. Individual HA needles or small groups then attached on micron-sized titania particles or dispersed among them. Furthermore, it is noted that, compared to the 5-10 nm titania particles, the P25 particles formed the coatings with less-aggregated structural feature (Fig. 3f).

The specific surface area of the as-sprayed coatings is shown in Fig. 4. The pure titania coating, pure HA coating, and P25 coating showed the value of 113.1, 81.5, and 54.6 m^2/g, respectively. Obviously the smallest particle size (5-10 nm) accounts for the highest specific surface area value of the pure titania coating, even though the aggregation is remarkable. The addition of HA reduced the specific surface area of both the titania coatings (5-10 nm in particle size) and the P25 coatings. The specific surface area of the titania-10 wt.% HA coating and the P25-10 wt.% HA coating is 110.6 and 53.1 m^2/g, exhibiting tiny lessening compared to the pure titania coatings. This is likely caused by constrained aggregation of the nano titania particles by HA.
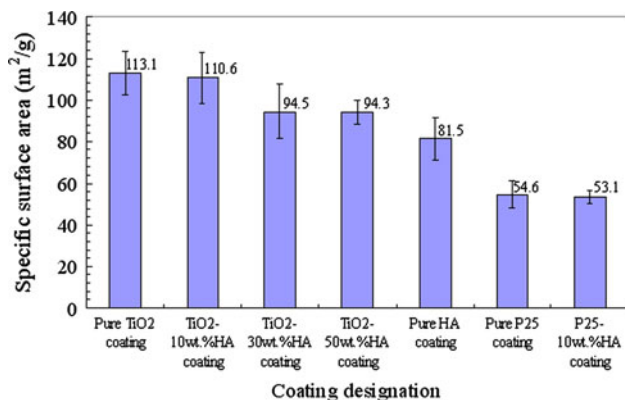
Fig. 4 Specific surface area values of the coatings as measured by the N$_2$-BET approach. For each sample, five specimens were measured for an average value

3.2 Bacteria Adhesion on the Coatings

After being incubated in bacteria solution (5 × 10^7 CFU/ml) for 6 h, the *E. coli* bacteria were fixed on the coating surfaces. In this case, *E. coli* was allowed to interact with the coatings for a relatively long duration and the number of the bacteria observed on the surfaces is a direct evidence of adherence behavior of the bacteria. SEM view shown in Fig. 5 clearly suggests that the number of *E. coli* on the surface of pure TiO$_2$ coatings is much less than that on the surface of the coatings containing HA. The number of the bacteria adhered on the coating surfaces after incubation of 6 h was determined following the approach reported in other studies (Ref 43, 44) by counting the bacteria from the SEM images. As shown in Fig. 6, consistent results are obvious that increase in HA content is accompanied with enhanced adherence of the bacteria. As expected, *E. coli* preferably adheres to HA, and the number of the adherent bacteria on the pure HA coatings is nine times more than those on the pure titania coating. Bacterial preference to HA was also evidenced by the selective adherence of the bacteria on HA needles/sheets in the composite coatings, which can be clearly observed from the further enlarged topographical view of the P25-10 wt.% HA coating (Fig. 5f). The bacteria attach mainly on or around HA needles/sheets, instead of on P25 particles. Bacterial adhesion to a material surface can usually be described as a two-phase process that occurs between bacteria and material surfaces, namely phase one (physicochemical interactions) and phase two (molecular and cellular interactions). In the second phase of adhesion, molecular reactions between bacterial surface structures and substrate surfaces become predominant (Ref 45). A number of studies have suggested that cell surface polysaccharides and proteins act as bacterial adhesions (Ref 46, 47). It is well known that HA has a good affinity to proteins and lipids, the addition of HA into titania coatings could certainly promote the bacterial adhesion. Fibrillar structures at the surface of various streptococci were believed to contribute to a better adhesion onto HA substrate (Ref 48). As mentioned above, individual HA needles or small groups attached on micron-sized titania particles or dispersed well among them. Most of the bacteria attached on HA also contact with titania. HA in the coatings therefore acts as bait attracting approaching of bacteria and simultaneously pushes them to titania. On the other hand, HA is capable of attracting adsorption of bacteria at night and in the places where no light is available, making mass bacteria-killing possible by the nano titania when light becomes accessible. Incorporation of HA into titania is therefore expected to possess a better antibacterial performance in terms of efficiency.

3.3 Photocatalytic Activity and Bacteria-Killing Performances of the Coatings

Photocatalytic performance of the TiO$_2$ and TiO$_2$/HA coatings was evaluated by degrading MB under UV irradiation. Before irradiation, the solution was stirred continuously in dark for 1 h to ensure adsorption/desorption
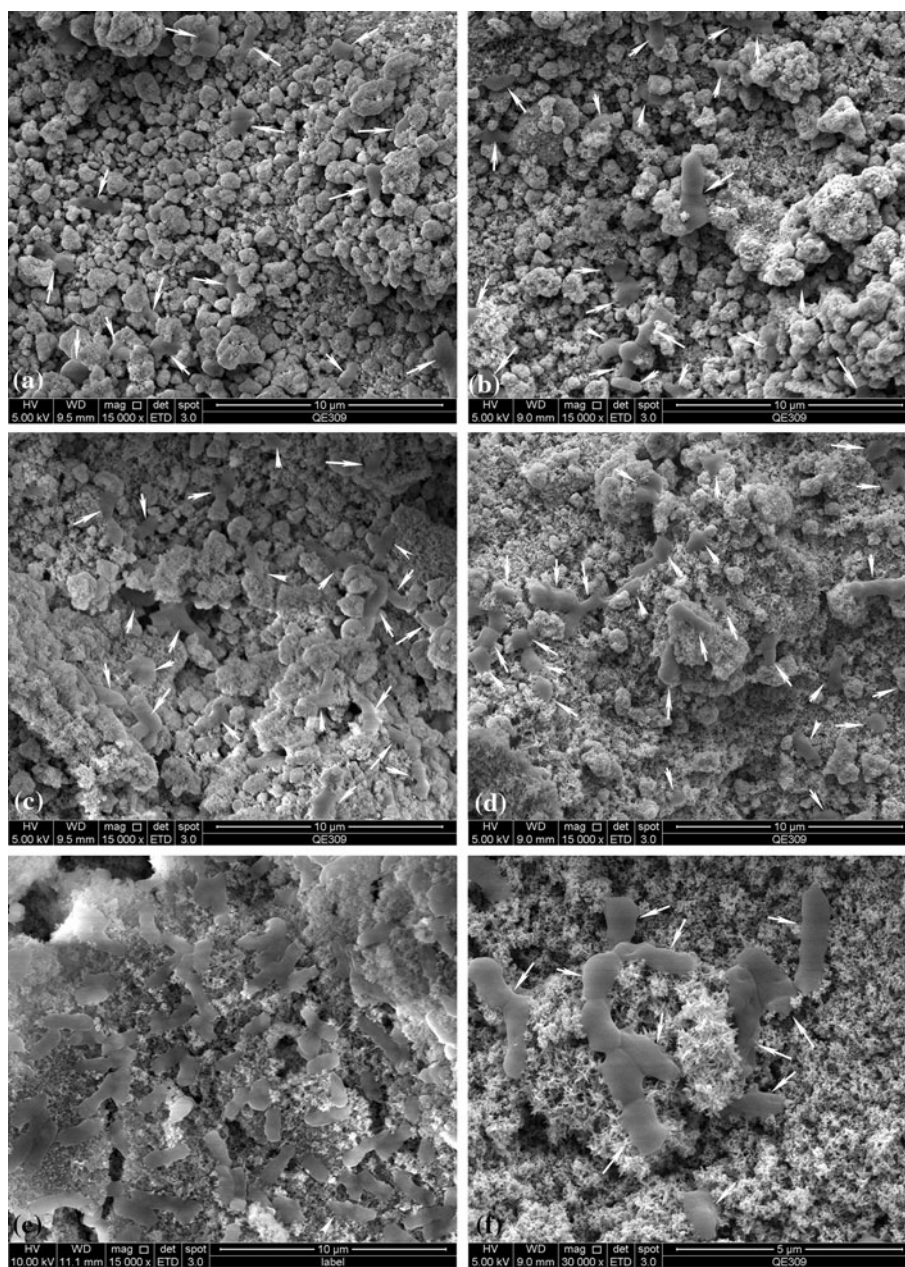
Fig. 5 Typical SEM photographs taken from the surfaces of the coatings after incubation in bacteria-containing media for 6 h showing clear adherence of *E. coli* bacteria on (a) the pure titania coating, (b) the titania-10 wt.% HA coating, (c) the titania-30 wt.% HA coating, (d) the titania-50 wt.% HA coating, (e) the pure HA coating, and (f) the P25-10 wt.% HA coating. The white arrows point to the adhered *E. coli*, and the *E. coli* bacteria were almost interconnected together on the surface of the pure HA coating (e)

equilibrium. The variation of the photodegradation of MB under the UV irradiation is shown in Fig. 7. It clearly illustrates that degradation was enhanced by elongated UV exposure and the decomposition rate (as revealed by the slope) decreased with the increase in reaction time. After 5.5 h degradation, the pure TiO_2 coating showed 61% degradation of MB. On the contrary, the pure HA coating and 316L plate showed neglectable photocatalytic behavior. However, surprisingly, the HA addition gave rise to further enhanced photocatalytic properties,

10 wt.% HA accomplished the best enhancement. After 6.5 h exposure, the coatings containing 10 wt.% HA, 30 wt.% HA, and 50 wt.% HA exhibit 86.8, 81.2, and 76.4% degradation of MB, respectively. Apart from the high adsorption property of HA, the well-dispersed titania particles (less aggregation) in the coatings, which means higher specific surface area, should be mainly responsible for the promoted photocatalytic activity. For the P25 coating, 91% of MB was degraded after 6.5 h incubation, which is much higher than the coatings made from the
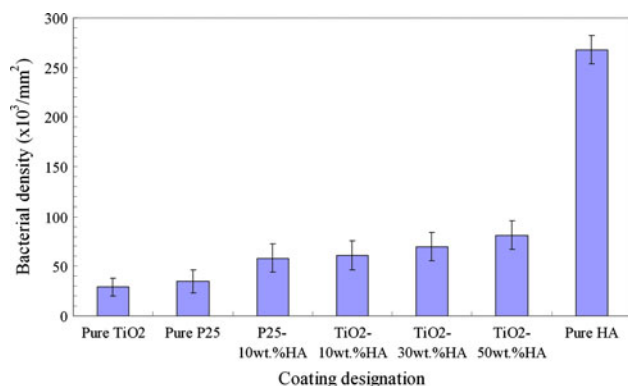
Fig. 6 Bacterial density as determined by statistical counting of the *E. coli* adhered on the surfaces of the coatings suggesting preferred adherence of the bacteria on HA-containing coatings. Digital images were taken randomly from at least five locations for each sample, and the number of the bacteria in each image was counted for averaged value
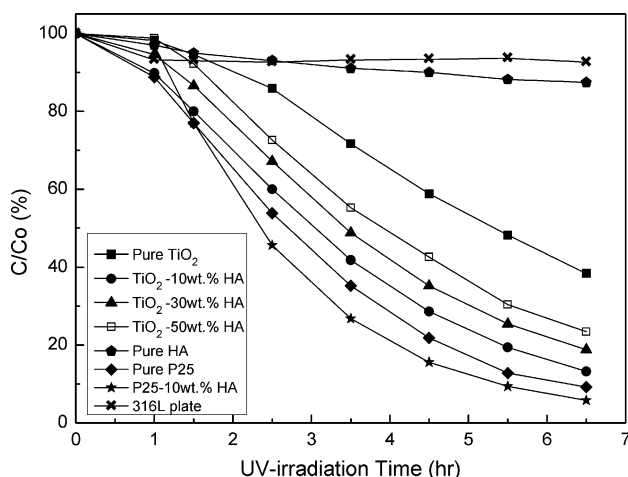
Fig. 7 Removal efficiency of MB by the coatings as represented by relative MB concentration C/Co vs. irradiation time. Co and C are the initial MB concentration and concentration at irradiation time *t* (h), respectively

titania of 5-10 nm in size. SEM characterization of the surfaces of the P25 coating (Fig. 3f) already showed less aggregation of the particles, favoring better contact of the coating with MB, and hence greater degradation. The coating, P25-10 wt.% HA coating, showed the highest degradation rate for MB, 94.2%. In order to further elucidate the photocatalytic behavior of the coatings, their wettability was also investigated. The contact angles of deionized distilled water droplet on the surfaces of the coatings were measured (data not shown). All the coatings showed a contact angle of ~10°, indicating their excellent hydrophilic performances for photocatalytic applications. No obvious differences in wettability were found for the coatings. In addition, electrostatic surface potentials of the coatings were also measured and no obvious differences were observed. It is known that surface charge and hydrophobicity properties of material affect bacterial adhesion on it (Ref 49). In this study, it is noted that the

addition of HA did not trigger obvious changes in surface charge and hydrophobicity properties of the coatings. In addition, extinguishment of *E. coli* bacteria adhered on the surfaces of the titania-based coatings was achieved by illumination of UV. It showed that after 2.5 h, the *E. coli* attached were all killed, which has been evidenced by SEM observation (data not shown). The bacteria attached on the pure HA coatings remain intact with no damage in their outer membrane. Similar phenomenon was observed for the *E. coli* absorbed on the uncoated plates as those absorbed on the HA coatings. Usually the photokilling reaction is initiated by a partial decomposition of the outer membrane of the bacterium, followed by disordering of its cytoplasmic membrane, resulting in ultimate cell death (Ref 50). Mechanism of the UV induced killing of *E. coli* on the titania-HA coatings is yet under investigation.

It was previously suggested that smaller crystallite size leads to higher rate of photocatalytic reaction (Ref 51). According to this study, however, it seems that the particle size is not the only decisive variable that accounts for the extent to which photocatalytic effect can be made. As shown in Fig. 3, aggregation of 5-10 nm titania particles was much severe compared to the P25 particles in their coatings, the specific surface area of the pure 5-10 nm titania coatings doubled that of the P25 coatings. It was expected that the pure 5-10 nm titania coatings might have a better photocatalytic activity. However, instead, the P25 coatings exhibited better performance (91% degradation of MB for the P25 coating and 61% for the 5-10 nm titania coating). In general, with a smaller particle size, the number of active surface sites increases, and so does the surface charge carrier transfer rate in photocatalysis (Ref 52). However, when particle size becomes extremely small (i.e. several nanometers in diameter), surface recombination becomes to be an important process (Ref 53-55). In the regime of ultrafine particle size, most of the e^-/h^+ pairs are generated sufficiently close to the surface. They may quickly reach the surface, and undergo rapid surface recombination due mainly to abundant surface trapping sites and the lack of driving force for e^-/h^+ pair separation (Ref 52). This phenomenon offsets the benefits from the ultrahigh surface area of nanocrystalline TiO_2 which is why an optimal value of 10 nm for pure TiO_2 photocatalyst was reported (Ref 56). The relatively low photocatalytic activity of the 5-10 nm titania coating in our study verifies well the above theory. In addition, it must be pointed out that ~120 ppm or 0.012 at.% of Fe^{3+} was detected in Degussa P25. The doping of transition metal such as Fe^{3+} facilitates trapping of electrons to inhibit electron-hole recombination during irradiation and decrease in charge carriers recombination results in enhanced photoactivity (Ref 57). It was reported that the high photoreactivity of Degussa P25 is due to its high crystallinity and the minor Fe^{3+} doping (Ref 52). Furthermore, some researchers suggested that the mixed composition of anatase and rutile was also partially responsible for Degussa P25's high photocatalytic reactivity (Ref 58). Therefore, taking into account the preferred attachment of bacteria on HA-containing coating,

flame-sprayed Degussa P25-10 wt.% HA or ~10 nm-titania-10 wt.% HA coatings might be the best choice as the photocatalyst for enhanced recruitment and subsequent killing of bacteria in a variety of antibacterial applications.

4. Conclusions

The nanostructured titania coatings with addition of HA (10, 30, 50 wt.%) have been successfully fabricated by suspension flame spraying. TiO_2 and HA retained their original nano features with no detectable signs of melting during the deposition. HA effectively inhibited phase transition of titania from anatase to rutile and restrained the aggregation of the nanosized TiO_2 particles. TiO_2-10 wt.% HA coatings yield the best photocatalytic performance compared with the photodegradation of MB. Bacterial adhesion tests proofed that the addition of HA facilitates the adsorption of *E. coli* bacteria on the surfaces of the coatings, suggesting the great potential of the composite coatings for antibacterial applications for water disinfection and air purification.

Acknowledgment

References

1. A. Fujishima and K. Honda, Electrochemical Photolysis of Water at a Semiconductor Electrode, *Nature*, 1972, **238**, p 37-38
2. W.W. Zhang, Y.Q. Chen, S.Q. Yu, S.G. Chen, and Y.S. Yin, Preparation and Antibacterial Behavior of Fe^{3+}-Doped Nanostructured TiO_2 Thin Films, *Thin Solid Films*, 2008, **516**, p 4690-4694
3. D.M.A. Alrousan, P.S.M. Dunlop, T.A. McMurray, and J.A. Byrne, Photocatalytic Inactivation of *E. coli* in Surface Water Using Immobilised Nanoparticle TiO_2 Films, *Water Res.*, 2009, **43**, p 47-54
4. A. Fujishima, X.T. Zhang, and D.A. Tryk, TiO_2 Photocatalysis and Related Surface Phenomena, *Surf. Sci. Rep.*, 2008, **63**, p 515-582
5. Y. Bessekhouad, D. Robert, and J.V. Weber, Preparation of TiO_2 Nanoparticles by Sol-Gel Route, *Int. J. Photoenergy*, 2003, **5**, p 153-158
6. T. Matsunaga, R. Tomoda, T. Nakajima, and H. Wake, Photoelectrochemical Sterilization of Microbial Cells by Semiconductor Powders, *FEMS Microbiol. Lett.*, 1985, **29**, p 211-214
7. O.K. Dalrymple, E. Stefanakos, M.A. Trotz, and D.Y. Goswami, A Review of the Mechanisms and Modeling of Photocatalytic Disinfection, *Appl. Catal. B Environ.*, 2010, **98**, p 27-38
8. H.F. Wang, Z.Q. Wang, H.X. Hong, and Y.S. Yin, Preparation of Cerium-Doped TiO_2 Film on 304 Stainless Steel and Its Bactericidal Effect in the Presence of Sulfate-Reducing Bacteria (SRB), *Mater. Chem. Phys.*, 2010, **124**, p 791-794
9. Y. Liu, X.L. Wang, F. Yang, and X.R. Yang, Excellent Antimicrobial Properties of Mesoporous Anatase TiO_2 and Ag/TiO_2 Composite Films, *Microporous Mesoporous Mater.*, 2008, **114**, p 431-439
10. T. Nonami, H. Hase, and K. Funakoshi, Apatite-Coated Titanium Dioxide Photocatalyst for Air Purification, *Catal. Today*, 2004, **96**, p 113-118
11. L.E. McNamara, T. Sjöström, K.E. Burgess, J.J. Kim, E. Liu, S. Gordonov, P.V. Moghe, R.M. Meek, R.O. Oreffo, B. Su, and M.J. Dalby, Skeletal Stem Cell Physiology on Functionally Distinct Titania Nanotopographies, *Biomaterials*, 2011, **32**, p 7403-7410
12. K. Ozeki, J.M. Janurudin, H. Aoki, and Y. Fukui, Photocatalytic Hydroxyapatite/Titanium Dioxide Multilayer Thin Film Deposited onto Glass Using an RF Magnetron Sputtering Technique, *Appl. Surf. Sci.*, 2007, **253**, p 3397-3401
13. A. Nakajima, K. Takakuwa, Y. Kameshima, M. Hagiwara, S. Sato, Y. Yamamoto, N. Yoshida, T. Watanabe, and K. Okada, Preparation and Properties of Titania-Apatite Hybrid Films, *J. Photochem. Photobiol. A Chem.*, 2006, **177**, p 94-99
14. M. Uzunova-Bujnova, R. Todorovska, M. Milanova, R. Kralchevska, and D. Todorovsky, On the Spray-Drying Deposition of TiO_2 Photocatalytic Films, *Appl. Surf. Sci.*, 2009, **256**, p 830-837
15. M.E. Fabiyi and R.L. Skelton, Photocatalytic Mineralisation of Methylene Blue Using Buoyant TiO_2-Coated Polystyrene Beads, *J. Photochem. Photobiol. A*, 2000, **132**, p 121-128
16. D.S. Kim and Y.S. Park, Photocatalytic Decolorization of Rhodamine B by Immobilized TiO_2 onto Silicone Sealant, *Chem. Eng. J.*, 2006, **116**, p 133-137
17. A. Fernandez, G. Lassaletta, V.M. Jimenez, A. Justo, A.R.G. Elipe, J.M. Herrmann, H. Tahiri, and Y. Ait-Ichou, Preparation and Characterization of TiO2 Photocatalysts Supported on Various Rigid Supports (Glass, Quartz and Stainless Steel). Comparative Studies of Photocatalytic Activity in Water Purification, *Appl. Catal. B*, 1995, **7**, p 49-63
18. Y. Chen, E. Stathatos, and D.D. Dionysiou, Microstructure Characterization and Photocatalytic Activity of Mesoporous TiO_2 Films with Ultrafine Anatase Nanocrystallites, *Surf. Coat. Technol.*, 2008, **202**, p 1944-1950
19. Y. Li, X. Li, J. Li, and J. Yin, Photocatalytic Degradation of Methyl Orange by TiO_2-Coated Activated Carbon and Kinetic Study, *Water Res.*, 2006, **40**, p 1119-1126
20. M. Kubo, H. Fukuda, X.J. Chua, and T. Yonemoto, Kinetics of Ultrasonic Degradation of Phenol in the Presence of Composite Particles of Titanium Dioxide and Activated Carbon, *Ind. Eng. Chem. Res.*, 2007, **46**, p 699-704
21. C. Kuo, Y. Tseng, C. Huang, and Y. Li, Carbon-Containing Nano-Titania Prepared by Chemical Vapor Deposition and Its Visible-Light-Responsive Photocatalytic Activity, *J. Mol. Catal. A*, 2007, **270**, p 93-100
22. M.G. Nolan, M.E. Pemble, D.W. Sheel, and H.M. Yates, One Step Process for Chemical Vapour Deposition of Titanium Dioxide Thin Films Incorporating Controlled Structure Nanoparticles, *Thin Solid Films*, 2006, **515**, p 1956-1962
23. L. Lei, H.P. Chu, X. Hu, and P.L. Yue, Preparation of Heterogeneous Photocatalyst (TiO2/Alumina) by Metallo-Organic Chemical Vapor Deposition, *Ind. Eng. Chem. Res.*, 1999, **38**, p 3381-3385
24. S. Karuppuchamy, K. Nonomura, T. Yoshida, T. Sugiura, and H. Minoura, Cathodic Electrodeposition of Oxide Semiconductor Thin Films and Their Application to Dye-Sensitized Solar Cells, *Solid State Ion.*, 2002, **151**, p 19-27
25. M.S. Djosic, V.B. Miskovic-Stankovic, D.T. Janackovic, Z.M. Kacarevic-Popovic, and R.D. Petrovic, Electrophoretic Deposition and Characterization of Boehmite Coatings on Titanium Substrate, *Colloids Surf. A*, 2006, **274**, p 185-191
26. S. Liu and X. Chen, Preparation and Characterization of a Novel Activated Carbon-Supported N-Doped Visible Light Response Photocatalyst (TiO2-xNy/AC), *Technol. Biotechnol.*, 2007, **82**, p 453-459
27. H. Herman, S. Sampath, and R. McCune, Thermal Spray: Current Status and Future Trends, *MRS Bull.*, 2000, **25**, p 17-25
28. A. Killinger, R. Gadow, and G. Mauer, Review of New Developments in Suspension and Solution Precursor Thermal Spray Processes, *J. Therm. Spray Technol.*, 2011, **20**, p 677-695
29. J. Yuan, Q. Zhan, Q. Lei, S. Ding, and H. Li, Fabrication and Characterization of Hybrid Micro/Nano-Structured Hydrophilic Titania Coatings Deposited by Suspension Flame Spraying, *Appl. Surf. Sci.*, 2012, **258**, p 6672-6678
30. F.-L. Toma, L.M. Berger, D. Jacquet, D. Wicky, I. Villaluenga, Y.R. de Miguel, and J.S. Lindeløv, Comparative Study on the Photocatalytic Behaviour of Titanium Oxide Thermal Sprayed

Coatings from Powders and Suspensions, *Surf. Coat. Technol.*, 2009, **203**, p 2150-2156

31. F.-L. Toma, G. Bertrand, D. Klein, C. Coddet, and C. Meunier, Nanostructured Photocatalytic Titania Coatings Formed by Suspension Plasma Spraying, *J. Therm. Spray Technol.*, 2006, **15**, p 587-592

32. F.-L. Toma, G. Bertrand, S. Begin, C. Meunier, O. Barres, D. Klein, and C. Coddet, Microstructure and Environmental Functionalities of TiO2-Supported Photocatalysts Obtained by Suspension Plasma Spraying, *Appl. Catal. B Environ.*, 2006, **68**, p 74-84

33. S.W.K. Kweh, K.A. Khor, and P. Cheang, The Production and Characterization of Hydroxyapatite (HA) Powders, *J. Mater. Process. Technol.*, 1999, **90**, p 373-377

34. R.A. Young, *The rietveld method*, Oxford University Press, Oxford, 1995

35. N. George, M. Mahon, and A. McDonald, Bactericidal Performance of Flame-Sprayed Nanostructured Titania-Copper Composite Coatings, *J. Therm. Spray Technol.*, 2010, **19**, p 1042-1053

36. M. Bozorgtabar, M. Rahimipour, and M. Salehi, Effect of Thermal Spray Processes on Anatase-Rutile Phase Transformation in Nano-Structured TiO$_2$ Photo-Catalyst Coatings, *Surf. Eng.*, 2010, **26**, p 422-427

37. X.L. Tan, Q.H. Fan, X.K. Wang, and B. Grambow, Eu(III) Sorption to TiO2 (Anatase and Rutile): Batch, XPS, and EXAFS Studies, *Environ. Sci. Technol.*, 2009, **43**, p 3115-3121

38. T.F. Stoica, C. Morosanu, A. Slav, T. Stoica, P. Osiceanu, C. Anasttasescu, M. Gartner, and M. Zaharescu, Hydroxyapatite Films Obtained by Sol-Gel and Sputtering, *Thin Solid Films*, 2008, **516**, p 8112-8116

39. N. Ohtsu, N. Masahashi, Y. Mizukoshi, and K. Wagatsuma, Hydrocarbon Decomposition on a Hydrophilic TiO$_2$ Surface by UV Irradiation: Spectral and Quantitative Analysis Using In situ XPS Technique, *Langmuir*, 2009, **25**, p 11586-11591

40. F.X. Ye, A. Ohmori, T. Tsumura, K. Nakata, and C.J. Li, Microstructural Analysis and Photocatalytic Activity of Plasma-Sprayed Titania-Hydroxyapatite Coatings, *J. Therm. Spray Technol.*, 2007, **16**, p 776-782

41. D.A.H. Hanaor and C.C. Sorrell, Review of the Anatase to Rutile Phase Transformation, *J. Mater. Sci.*, 2011, **46**, p 855-874

42. U. Cernigoj, U.L. Stangar, P. Trebse, U.O. Kraxovec, and S. Gross, Photocatalytically Active TiO$_2$ Thin Films Produced by Surfactant-Assisted Sol-Gel Processing, *Thin Solid Films*, 2006, **495**, p 327-332

43. J. Tsibouklis, M. Stone, A.A. Thorpe, P. Graham, T.G. Nevell, and R.J. Ewen, Inhibiting Bacterial Adhesion onto Surfaces: the Non-Stick Coating Approach, *Int. J. Adhes. Adhes.*, 2000, **20**, p 91-96

44. Y.L. Jeyachandran, S. Venkatachalam, B. Karunagaran, S.K. Narayandass, D. Mangalaraj, C.Y. Bao, and C.L. Zhang, Bacterial Adhesion Studies on Titanium, Titanium Nitride And Modified Hydroxyapatite Thin Films, *Mater. Sci. Eng. C Mater. Biol. Appl.*, 2007, **27**, p 35-41

45. Y.H. An and R.J. Friedman, Concise Review of Mechanisms of Bacterial Adhesion to Biomaterial Surfaces, *J. Biomed. Mater. Res. B*, 1998, **43**, p 338-348

46. K.D. Kroncke, I. Orskov, F. Orskov, B. Jann, and K. Jann, Electron-Microscopic Study of Compression of Adhesive Protein Capsules and Polysaccharide Capsules in *Escherichia coli*, *Infect. Immun.*, 1990, **58**, p 2710-2714

47. M. Fletcher and G.D. Floodgate, An Electron-Microscopic Demonstration of an Acidic Polysaccharide Involved in the Adhesion of a Marine Bacterium to Solid Surfaces, *J. Gen. Microbiol.*, 1973, **74**, p 325-334

48. G.N. Phillips, P.E. Flicker, C. Cohen, B.N. Manjula, and V.A. Fischetti, Streptococcal M Protein: Alpha-Helical Coiled-Coil Structure and Arrangement on the Cell Surface, *Proc. Natl. Acad. Sci. U. S. A.*, 1981, **78**, p 4689-4693

49. L. Ploux, A. Ponche, and K. Anselme, Bacteria/Material Interfaces: Role of the Material and Cell Wall Properties, *J. Adhes. Sci. Technol.*, 2010, **24**, p 2165-2201

50. K. Sunada, T. Watanabe, and K. Hashimoto, Studies on Photokilling of Bacteria on TiO$_2$ Thin Film, *J. Photochem. Photobiol. A Chem.*, 2003, **156**, p 227-233

51. C. Lee, H. Choi, C. Lee, and H. Kim, Photocatalytic Properties of Nano-Structured TiO$_2$ Plasma Sprayed Coating, *Surf. Coat. Technol.*, 2003, **173**, p 192-200

52. Z.B. Zhang, C.C. Wang, R. Zakaria, and J.Y. Ying, Role of Particle Size in Nanocrystalline TiO2-Based Photocatalysts, *J. Phys. Chem. B*, 1998, **102**, p 10871-10878

53. N. Serpone, D. Lawless, R. Khairlutdinov, and E. Pelizzetti, Subnanosecond Relaxation Dynamics in TiO$_2$ Colloidal Sols (Particle Sizes Rp = 1.0-13.4 nm)-Relevance to Heterogeneous Photocatalysis, *J. Phys. Chem.*, 1995, **99**, p 16655-16661

54. M.A. Hines and P. Guyot-Sionnest, Synthesis and Characterization of Strongly Luminescing ZnS-Capped CdSe Nanocrystals, *J. Phys. Chem.*, 1996, **100**, p 468-471

55. A.R. Kortan, R. Hull, R.L. Opila, M.G. Bawendi, M.L. Steigerwald, P.J. Carroll, and L.E. Brus, Nucleation and Growth of Cadmium Selenide on Zinc Sulfide Quantum Crystallite Seeds, and Vice Versa, in Inverse Micelle Media, *J. Am. Chem. Soc.*, 1990, **112**, p 1327-1332

56. C.C. Wang, Z.B. Zhang, and J.Y. Ying, Photocatalytic Decomposition of Halogenated Organics Over Nanocrystalline Titania, *Nanostruct. Mater.*, 1997, **9**, p 583-586

57. M.I. Litter and J.A. Navio, Photocatalytic Properties of Iron-Doped Titania Semiconductors, *J. Photochem. Photobiol. A*, 1996, **98**, p 171-181

58. R.I. Bickley, T. Gonzalez-Carreno, J.S. Lees, L. Palmisano, and R.J.D. Tilley, A Structural Investigation of Titanium Dioxide Photocatalysts, *J. Solid State Chem.*, 1991, **92**, p 178-190